IVYSPRING INTERNATIONAL PUBLISHER

International Journal of Biological Sciences

2027; 23(1): 270-287. doi: 10.7150/ijbs.138139

Research Paper

A CBS3-targeting direct AMPK activator ameliorates Alzheimer's disease pathology and cognitive decline

Kyung-Hwa Jeon[1,2,†], Hyunji Jo[1,†], Soyeon Cho[3,†], Jae-Ho Shin[4], Seojeong Park[1], Kyu-Yeon Jun[1], Seojeong Kim[1], Seung Hee Seo[1], Soo-Yeon Hwang[1], Dabin Song[3], Yumi Son[3], Zhi Zheng[5], Hyunjeong Kim[3], Younghwa Na[4,✉], Eosu Kim[3,✉], and Youngjoo Kwon[1,2,6,✉]

1. College of Pharmacy, Graduate School of Pharmaceutical Sciences, Ewha Womans University, Seoul, 03760, Korea.
2. Graduate Program in Innovative Biomaterials Convergence, Ewha Womans University, Seoul 03760, Korea.
3. Department of Psychiatry, Institute of Behavioral Science in Medicine, Yonsei Metabolism-Dementia Research Institute, Brain Korea 21 Project for Medical Science, Yonsei University College of Medicine, Seoul, 03722, Korea.
4. College of Pharmacy, CHA University, Pocheon, 11160, Korea.
5. Department of Toxicology, School of Public Health, Xinxiang Medical University, Henan, China.
6. Graduate Program in Regulatory Science Convergence, Ewha Womans University, Seoul, 03760, Republic of Korea

†These authors equally contributed.

✉ Corresponding authors: Youngjoo Kwon; Tel: 82-2-3277-4653; Fax: 82-2-3277-2851; E-mail: ykwon@ewha.ac.kr. Eosu Kim; Tel: 82-2-2228-1620; Fax: 82-2-313-0891; Email: eosu.kim@yonsei.ac.kr. Younghwa Na; Tel: 82-31-8017-9416; Fax: 82-31-8017-9420; E-mail: yna7315@cha.ac.kr.

© 2027 The Author(s). This is an open access article distributed under the Creative Commons Attribution 4.0 International Licence, subject to the Publisher's Terms of Use at https://ivyspring.com/terms.

Received: 2026.05.21; Accepted: 2026.10.08; Published: 2027.01.01

Abstract

Alzheimer's disease (AD) is a multifactorial neurodegenerative disorder characterized by amyloid deposition, neuroinflammation, oxidative stress, and progressive cognitive decline. Although AMP-activated protein kinase (AMPK) has emerged as a key regulator of cellular energy homeostasis and neuronal function, most pharmacological activators act indirectly and may exacerbate metabolic stress under disease conditions, limiting their therapeutic utility. Here, we identified YE-06 as a direct AMPK activator that targets the CBS3 site of the AMPKγ subunit through a non-nucleotide-mimetic scaffold. Biochemical and cellular analyses demonstrate that YE-06 directly engages AMPK and promotes sustained activation through an LKB1-dependent mechanism. Functionally, YE-06 suppresses BACE1 expression and amyloidogenic processing, attenuates microglial inflammatory responses, and reduces oxidative stress via coordinated regulation of NF-κB and Nrf2 signaling pathways. In vivo, YE-06 improves cognitive performance in both intrahippocampal Aβ1–42-injected mice and 3xTg-AD mouse models without affecting locomotor activity. YE-06 also exhibits favorable pharmacological properties, including oral bioavailability and an acceptable safety profile.

Together, our findings identify YE-06 as a previously unrecognized direct AMPK activator and demonstrate that pharmacological activation of AMPK can modulate multiple pathological processes in AD. These results support direct AMPK activation as a potential disease-modifying therapeutic strategy for AD.

Keywords: Alzheimer's disease; AMP-activated protein kinase (AMPK); AMPKγ CBS3 site-targeting; direct AMPK activator; touchscreen-based behavioral test; cognitive function

Introduction

Alzheimer's disease (AD) is the most prevalent cause of dementia, characterized by a gradual decline in cognitive function. The two major neuropathological hallmarks of AD are β-amyloid (Aβ) plaques and tau-related neurofibrillary tangles. Recently, monoclonal antibodies targeting Aβ plaques or protofibrils have shown promise in modifying disease progression in patients with early-stage AD [1-3]. However, given the multifactorial nature of AD pathogenesis, there is a growing need to explore therapeutic targets beyond amyloid and tau, such as metabolic dysfunction, neuroinflammation, and

oxidative stress [4]. Accordingly, an increasing number of phase 3 drug candidates are now directed toward non-amyloid/non-tau mechanisms, with several aimed at modulating brain energy metabolism [5].

AMP-activated protein kinase (AMPK) is a master regulator of energy metabolism, consisting of a catalytic subunit (α1 or α2), a scaffold subunit (β1 or β2), and a regulatory subunit (γ1, γ2, or γ3). AMPK modulates energy homeostasis by sensing the cellular AMP/ADP-to-ATP ratio, thereby affecting glycolysis, fatty acid oxidation, and mitochondrial biogenesis. In addition to its metabolic function, AMPK also regulates aging-related cellular processes, including neuroinflammation, oxidative stress, and autophagy. Importantly, AMPK activity has been reported to decline during aging [6, 7], suggesting a potential link between reduced AMPK signaling and susceptibility to cognitive decline and AD [8].

As aging and metabolic impairment are primary risk factors of AD, AMPK has emerged as a promising therapeutic target for this disease. Indeed, mounting evidence implicates AMPK in AD pathogenesis, with various AMPK activators showing potential to attenuate AD-associated pathology in cellular and animal models [9-11]. Recent studies analyzing human brain disease networks and somatic mutation profiles have also identified AMPK as a critical regulatory node in AD pathogenesis [12, 13]. However, most currently available AMPK activators are indirect, functioning by increasing the AMP/ADP:ATP ratio through inhibition of the mitochondrial respiratory chain [14]. While this type of AMPK activation may be tolerated under normal physiological conditions, it may exacerbate cellular energy stress in aging or disease contexts [15-17]. These limitations highlight the need for direct AMPK activators that engage specific regulatory sites of the kinase complex, including the allosteric drug and metabolite (ADaM) site and AMP-binding site 3 within the γ subunit. Notably, despite ongoing efforts to develop direct AMPK activators, their practical therapeutic application remains limited.

To address these limitations, we sought to identify a direct AMPK activator capable of engaging regulatory nucleotide-binding sites within the AMPK complex. In the present study, we identify YE-06 as a novel small molecule that directly targets the CBS3 site of the AMPKγ subunit through a non-nucleotide-mimetic scaffold. Using biochemical, structural, and cellular approaches, we demonstrate that YE-06 directly activates AMPK and promotes sustained signaling through an LKB1-dependent mechanism. Functionally, AMPK activation by YE-06 suppressed BACE1 expression and amyloidogenic processing, attenuated microglial inflammatory responses and oxidative stress, and improved neuronal survival. Importantly, these molecular effects translated into significant improvements in cognitive performance in both $A\beta_{1-42}$-injected mice and 3xTg-AD mouse models. Together, these findings identify YE-06 as a previously unrecognized direct AMPK activator and highlight pharmacological activation of AMPK as a potential disease-modifying strategy for AD.

Material and Methods

Synthesis of YE-06

YE-06 was synthesized and its purity (96.1%) was confirmed by high-performance liquid chromatography (HPLC). Detailed information regarding the synthesis process, ^{1}H and ^{13}C nuclear magnetic resonance (NMR) spectral data, HPLC data, and liquid chromatography-high resolution mass spectroscopic data for YE-06 are provided in the Supplementary information.

Western blot analysis

Western blot analysis was performed as previously published [18]. Briefly, proteins were extracted using RIPA buffer (Cell Signaling Technology, Danvers, MA, USA) consisting of 1% protease inhibitor (GenDEPOT, Katy, USA) and protein concentrations were determined using a BCA protein assay kit (Thermo Fisher Scientific, Waltham, USA). After separation by SDS-PAGE, proteins were transferred onto a 0.2 μm PVDF membrane (Pall Life Science, New York, USA). Subsequently, membranes were blocked with 5% skim milk or 5% BSA and then incubated with specific primary antibodies followed by appropriate secondary antibodies. Protein bands were visualized using an ECL solution reagent (GE Healthcare, Chicago, USA) and detected using a ChemiDoc MP (Bio-rad, USA) equipped at Ewha Drug Development Research Core Center. The antibodies used in this study are listed in Table S1 & S3.

Real-time quantitative PCR and reverse transcription PCR

Total RNA was extracted using Tri-RNA reagent (FAVORGEN Biotech, Wien, Austria), and complementary DNA (cDNA) was synthesized using the PrimeScript™ RT reagent kit (Takara). Real-time quantitative PCR was performed with the SensiFAST™ SYBR No-ROX kit (Bioline, Memphis, TN, USA), utilizing the CFX96 Real-time PCR detection system (Bio-Rad, Hercules, USA; NFEC-2021-08-272451) equipped at Ewha Drug Development Research Core Center. The relative mRNA expression of target genes was determined with the comparative

Ct (ΔΔCt) quantification method, with normalization to GAPDH expression. For reverse transcription PCR, the EmeraldAmp® PCR Master Mix (Takara, Kyoto, Japan) was used in a final reaction volume of 50 μL, and PCR amplification was performed using the SimpliAmp™ Thermal Cycler (Thermo). PCR products were electrophoresed on a 1% agarose gel, stained in an EtBr solution, and visualized by transillumination with UV light. The sequences of primers used for RT–qPCR and reverse transcription PCR are listed in Table S2.

Animals and experimental groups

Male ICR mice (6 weeks old) were purchased from Central Laboratory Animal, Inc. (Seoul, Republic of Korea) for the $A\beta_{1-42}$ injection model. Male C57BL/6 mice (8 weeks old) were obtained from Orient Bio, Inc. (Seongnam, Republic of Korea) for the electrophysiology and compound C (Dorsomorphin; Santa Cruz Biotechnology, Santa Cruz, CA, USA) treatment experiments. Male and female transgenic 3xTg-AD mice (B6;129-Tg [APPSwe, tauP301L] 1Lfa *Psen1*^{tm1Mpm}/Mmjax; MMRRC Stock No. 34830-JAX; the Jackson Laboratory, Bar Harbor, ME, USA) were bred in-house for acute and chronic YE-06 treatment experiments. Animals were housed 1-5 per cage in a light-controlled room (lights on from 8:00 a.m. to 8:00 p.m.) with *ad libitum* access to food and water, at a temperature of 22 ± 3℃ and a humidity of 50 ± 20%. All experiments were conducted following the guidelines of the Institutional Animal Care and Use Committee (IACUC) of Yonsei University (Approval no. 2017-0088, 2021-0233).

We employed three distinct experimental cohorts to assess the behavioral effects of YE-06. Cohort 1 was designed for behavioral experiments with $A\beta_{1-42}$-injected mice. Male ICR mice were randomly assigned into one of six groups: (i) Control group: mice received intrahippocampal injection of artificial cerebrospinal fluid (ACSF), composed of 145 mM NaCl, 2.7 mM KCl, 12 mM $CaCl_2$, and 1.0 mM $MgCl_2$, and were orally administered saline. (ii) Aβ group: mice received intrahippocampal injections of $A\beta_{1-42}$ (Sigma-Aldrich, Cat No. SCP0038, MO, USA) and were orally administered saline. (iii) Donepezil group: mice received intrahippocampal injections of $A\beta_{1-42}$ and were orally administered donepezil at a dose of 1 mg/kg/day. (iv) YE-06 1 mg/kg group, (v) YE-06 10 mg/kg group, and (vi) YE-06 100 mg/kg group. In groups (iv)–(vi), mice received intrahippocampal injections of $A\beta_{1-42}$ and were orally administered YE-06 at the indicated doses. All oral treatments (saline, donepezil, or YE-06) were administered once daily. Behavioral experiments were conducted when the mice were 7–8 weeks of age. Cohort 2 was designated for touchscreen-based cognitive behavioral testing. Male C57BL/6 and male 3xTg-AD mice were subjected to food restriction to maintain their weight at 85–90% of their average free-feeding weight. All behavioral trainings in touchscreen chambers were conducted once a day for 5–7 days per week. Probe sessions were performed in 15-month-old C57BL/6 and 10-month-old 3xTg-AD mice. Cohort 3 was used for the novel object recognition test, using male and female 3xTg-AD mice. NOR testing was performed after 12 weeks of oral YE-06 treatment in 9- or 12-month-old mice. All experiments were conducted in accordance with the ARRIVE guidelines. Animals were randomly assigned to experimental groups. Animals that failed to meet predefined behavioral performance criteria or died unexpectedly during the study were excluded from the final analyses. The final number of mice included in each experiment is indicated in the corresponding figure legends. Touchscreen behavioral data were automatically recorded using the touchscreen software. For non-touchscreen behavioral experiments, video files were coded by an independent investigator before analysis, and behavioral scoring was performed blinded to treatment allocation.

Statistical analysis

The results of all experiments, except those involving animals, were expressed as the mean ± standard error of the mean (SEM). Statistical analyses were conducted using the Unpaired student's t-test, ordinary one-way, or two-way analysis of variance (ANOVA) followed by Tukey's multiple comparisons test with GraphPad Prism version 11.0.0 (Graphpad Software Inc, San Diego, CA, USA). Statistical analyses of animal experiment data were performed using R version 4.2.2 and GraphPad Prism version 11 (GraphPad Software Inc., San Diego, CA, USA). Data were analyzed using Student's t-test, one-way ANOVA followed by Dunnett's multiple comparisons test, or a two-way mixed-effects model followed by Dunnett's or Tukey's multiple comparisons test, as appropriate. Statistical significance was defined as $p < 0.05$.

Further information on methods

Further methodological details regarding in silico docking study, cell culture, plasmid transfection of AMPK wild-type and mutants, drug treatment in cells, AMPK kinase assay, cell viability assay, cellular thermal shift assay, immunofluorescence assay, subcellular fractionation, dot blot analysis, ELISA assay, DCFH-DA assay, RT-qPCR, NAD^+ and NADH quantification, ADP and ATP assay, $A\beta_{1-42}$ fibril synthesis and stereotaxic surgery, drug administration

protocols, Morris water maze test, passive avoidance test, rotarod test, vertical pole test, novel object recognition test, touchscreen behavioral assessment, brain slice preparation, electrophysiology recordings, measurement of acetylcholine (Ach) content and acetylcholinesterase (AChE) activity, TUNEL assay, mouse western blot, and mouse primary neuron culture are provided in the Supplementary Information.

Results

Transcriptomic analysis reveals coordinated suppression of AMPK signaling in the AD hippocampus

To establish the therapeutic relevance of targeting AMPK in AD, we analyzed publicly available datasets derived from hippocampal tissues of AD patients and non-demented controls. Differential gene expression analysis revealed significant alterations in AD samples (Figure 1A-B). Hallmark gene set enrichment analysis (GSEA) demonstrated broad negative enrichment across multiple biological processes involved in energy metabolism, cellular stress responses, and immune-related programs in AD hippocampi (Supplementary Figure S1). We next performed focused GSEA using curated AMPK-related gene sets. Notably, all AMPK-associated gene sets exhibited negative normalized enrichment scores (NESs) in AD patients, indicating coordinated downregulation of AMPK-dependent transcriptional programs (Figure 1C). To further define the relationship between AD-associated transcriptional changes and AMPK-related pathways, we integrated differentially expressed genes (DEGs) with AMPK-associated gene sets using a circos plot. This analysis demonstrated that multiple AD-associated DEGs were shared across functionally relevant AMPK-related gene sets, highlighting a convergent link between disease-associated transcriptional alterations and suppression of AMPK-regulated homeostatic networks (Figure 1D). Together, these findings support the rationale for pharmacological activation of AMPK as a therapeutic strategy in AD.

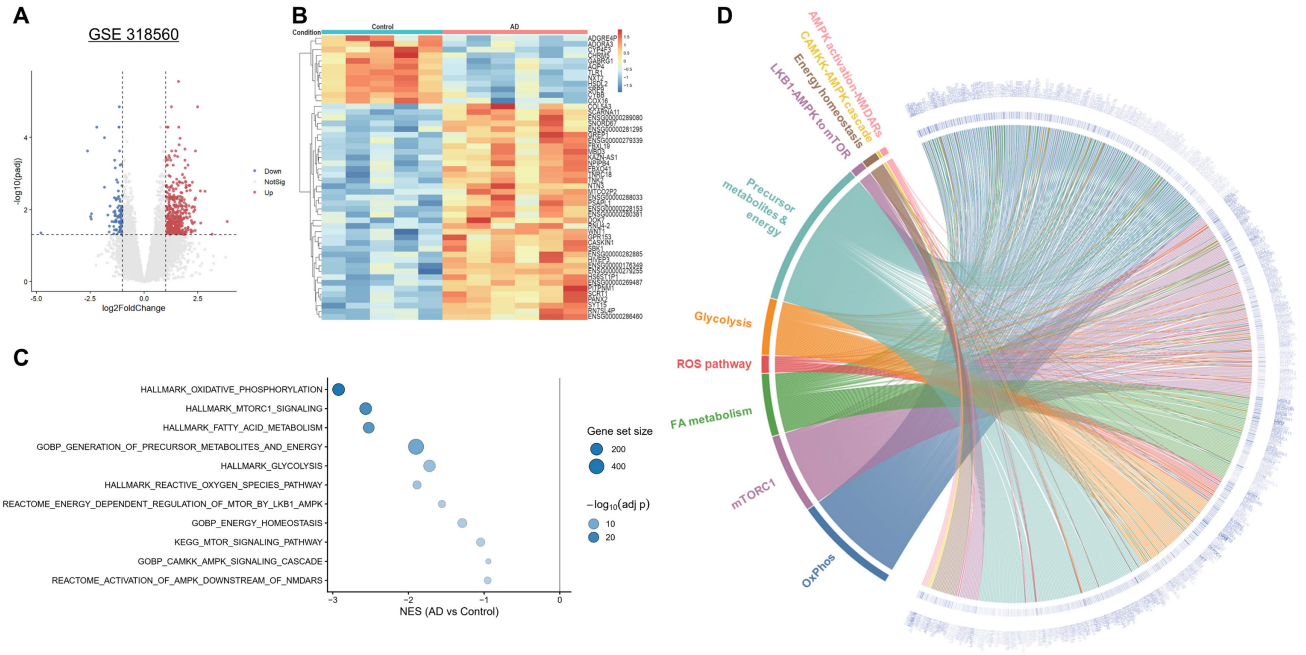


Figure 1. Transcriptomic analysis reveals suppression of AMPK-associated signaling in the Alzheimer's disease hippocampus. (A) Volcano plot showing differentially expressed genes (DEGs) in hippocampal tissues from patients with Alzheimer's disease (AD) compared with non-demented controls (GSE318560). Each dot represents a gene, plotted according to log_2FC and statistical significance (log10 adjusted p-value). **(B)** Heatmap of DEGs illustrating distinct transcriptional profiles between AD and control samples. **(C)** Gene set enrichment analysis (GSEA) of curated AMPK-related gene sets showing negative normalized enrichment scores (NESs) in AD samples. **(D)** Circos plot integrating AD-associated DEGs with AMPK-related gene sets. Gene nodes are connected to AMPK-related pathways, illustrating the transcriptomic association between disease-related gene expression changes and AMPK-regulated biological networks. Gene nodes are colored according to log_2FC in AD versus non-AD controls, and links indicate shared genes between the DEG list and individual AMPK-related pathways.

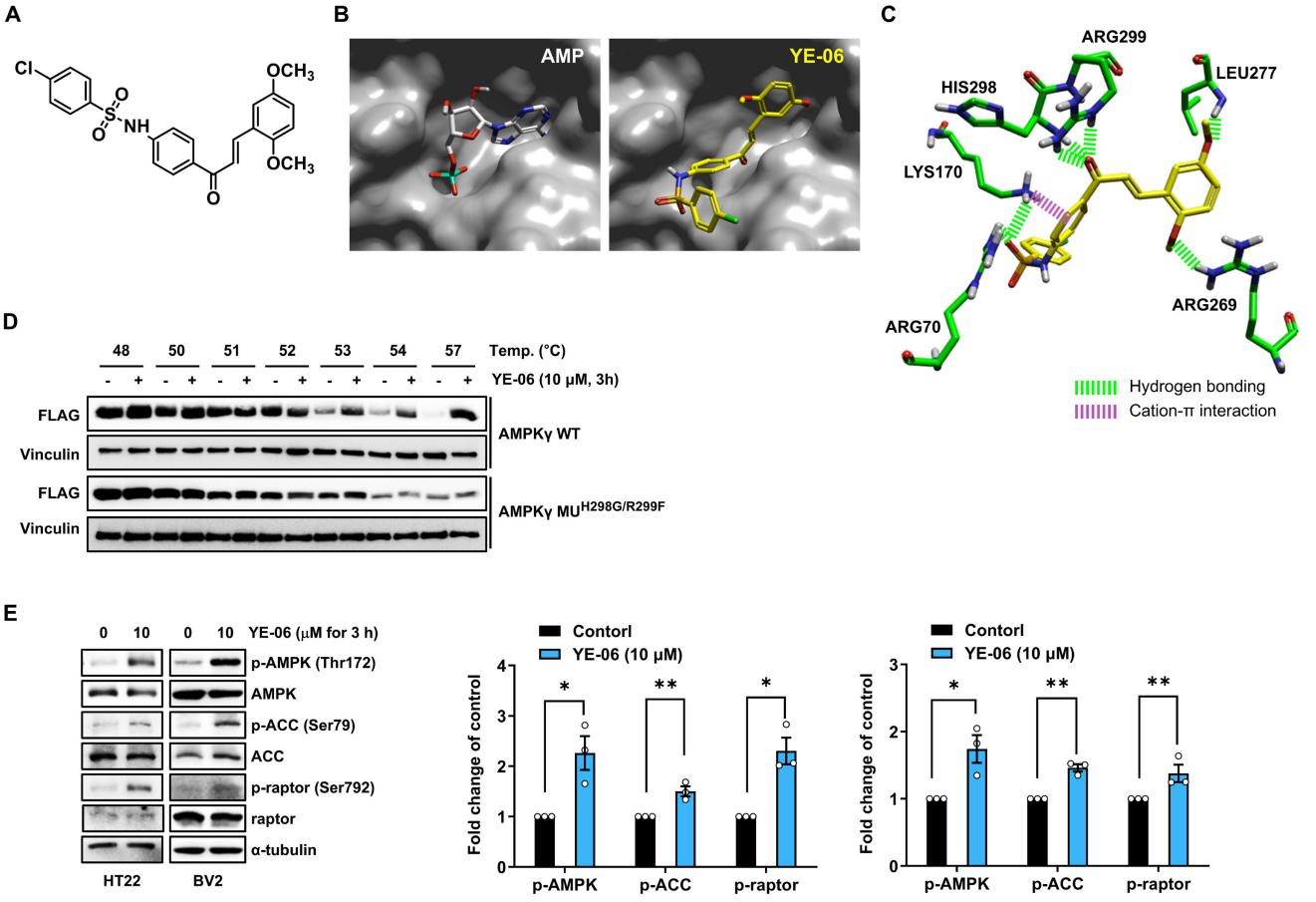


Figure 2. YE-06 directly binds to the AMPKγ subunit and activates AMPK signaling. (A) Chemical structure of YE-06. **(B)** Predicted binding mode of YE-06 within the AMP-binding site of the AMPKγ subunit. Molecular docking was performed using X-ray crystal structure (PDB ID: 4RER) and visualized using Flare™ software. **(C)** Detailed molecular interactions showing hydrogen bond formation between YE-06 and key residues within the CBS3 site of AMPKγ. **(D)** Cell thermal shift assay (CETSA) demonstrating increased thermal stability of AMPKγ in cells expressing wild-type (WT), but not mutant MU$^{H298G/R299F}$, followed by treatment with YE-06. **(E)** Western blot analysis showing increased phosphorylation of AMPK and downstream targets in HT22 and BV2 cells treated with YE-06. Data are presented as the mean ± SEM. Statistical significance was determined using a one-sample t-test against a theoretical mean of 1 (control level). *p < 0.05, **p < 0.01, ***p < 0.001.

YE-06 directly engages AMPKγ and promotes sustained AMPK activation

In our previous study, YE-06 was identified as a direct activator of AMPK (Figure 2A) [19]. To further define the molecular basis of this activation, we investigated the interaction between YE-06 and the AMPKγ subunit. Molecular docking analysis revealed that YE-06 formed hydrogen bonds with key residues at the CBS3 site of the AMPKγ subunit, overlapping with the interactions formed by the phosphate group of AMP (Figure 2B-C). To experimentally validate this direct interaction, we performed a cellular thermal shift assay (CETSA) using wild-type (WT) and mutant (MU$^{H298G/R299F}$) forms of AMPKγ. CETSA, a widely used label-free technique, monitors changes in thermal stability induced by ligand binding to endogenous target proteins within cells [20]. The results showed that YE-06 markedly increased the thermal stability of AMPKγ in cells expressing AMPKγ WT, whereas no stabilization was observed in cells expressing AMPKγ MU$^{H298G/R299F}$ (Figure 2D & Supplementary Figure S2A). These findings indicate that YE-06 directly binds to AMPKγ through interactions involving HIS298 and ARG299. Consistent with this mechanism, western blot analysis confirmed that YE-06 increased the levels of phosphorylated AMPK (p-AMPK, the activated form of AMPK) and its downstream targets, including phosphorylated acetyl-CoA carboxylase (p-ACC) and phosphorylated raptor (p-raptor), in HT22 neuronal cells and BV2 microglial cells (Figure 2E).

Because the AMPKγ subunit contains exchangeable nucleotide-binding sites, with CBS3 representing a key AMP-responsive regulatory site [21-23], we next assessed whether YE-06 functionally competes with AMP at this site. In an *in vitro* AMPK kinase assay using AMPK heterotrimers containing either α1 or α2, YE-06 showed no apparent α-isoform bias, unlike C2, a known direct AMPK activator (Supplementary Figure S2B) [24]. In addition, AMP did not further enhance AMPK activation beyond that induced by YE-06 alone (Supplementary Figure S2C), suggesting that YE-06 competes with AMP for binding to AMP-binding site 3 of AMPKγ under the tested

conditions. We next investigated whether upstream kinases contribute to YE-06-mediated AMPK activation [25, 26]. Inhibition of CaMKK2 with STO-609 did not affect YE-06-induced AMPK activation, indicating that CaMKK2 is not required for this process (Figure 3A). By contrast, in LKB1-deficient HeLa cells, YE-06 induced only transient AMPK activation, whereas ectopic expression of LKB1 prolonged YE-06-mediated AMPK activation (Figure 3B). Consistent with this, YE-06 increased the NAD^+/NADH ratio in N2a cells, and this effect was blocked by the Nampt inhibitor FK866 (Supplementary Figure S2D) [27]. Moreover, YE-06 significantly increased intracellular ATP levels and decreased the ADP/ATP ratio (Supplementary Figure S2E), indicating improved cellular energy status following YE-06 treatment. Immunofluorescence analysis further showed that YE-06 promoted the translocation of LKB1 from the nucleus to the cytoplasm (Figure 3C). Together, these findings suggest that YE-06 directly activates AMPK and that LKB1 contributes to maintaining this response, potentially through an AMPK–NAD+–SIRT1–LKB1 positive feedback axis associated with improved cellular energy homeostasis. Activation of AMPK is known to increase intracellular NAD+ levels, thereby activating the NAD^+-dependent deacetylase SIRT1, which in turn promotes LKB1 deacetylation and its nuclear export [27, 28]. This regulatory loop may reinforce AMPK signaling by facilitating LKB1-dependent phosphorylation of AMPK in the cytoplasm.

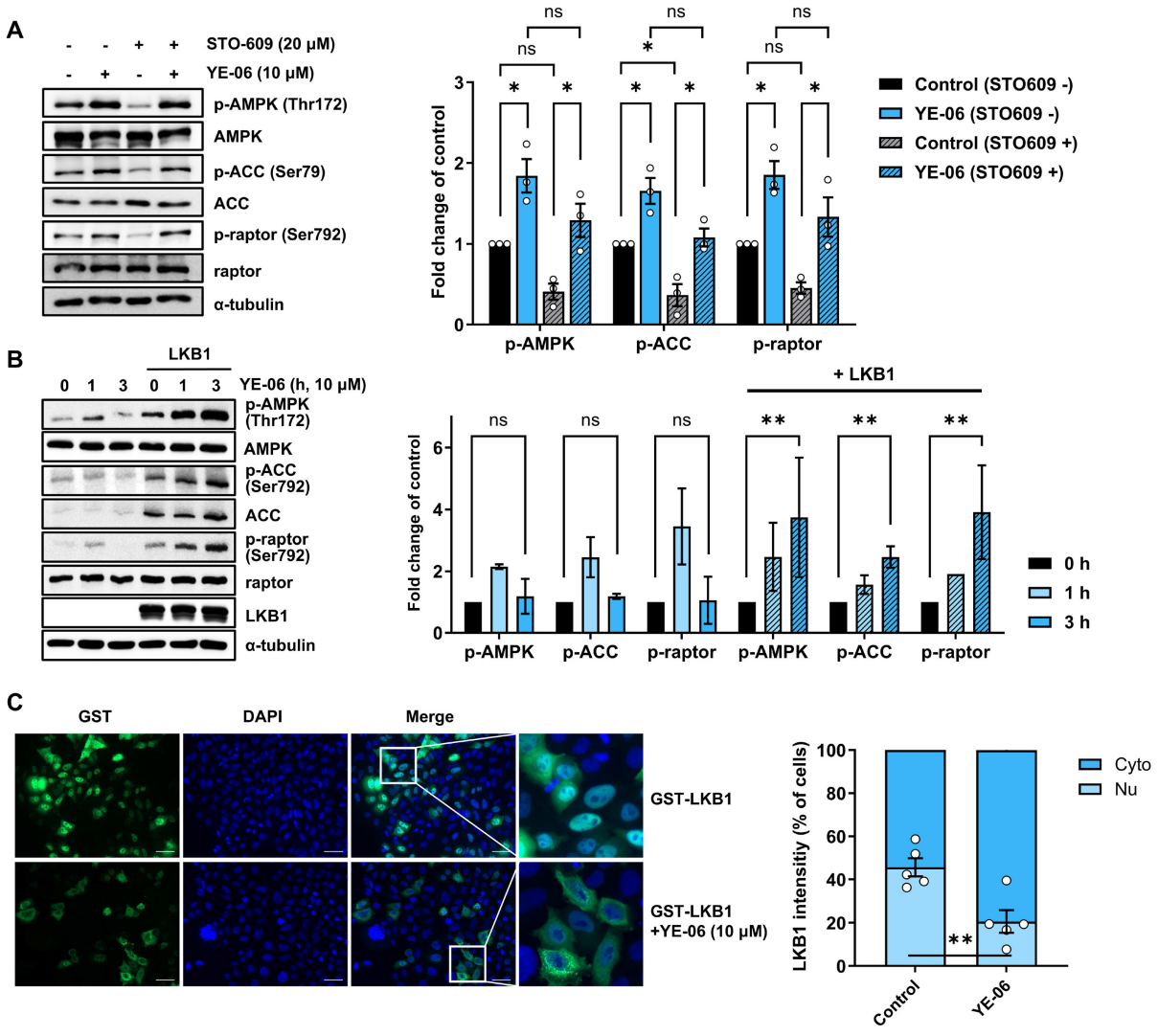


Figure 3. LKB1-dependent activation of AMPK by YE-06. (A) Western blot analysis showing that inhibition of CaMKK2 does not affect YE-06-induced AMPK activation in HT22 cells. HT22 cells were treated with YE-06 for 3 h with or without pretreatment of STO-609, a CaMKK2 inhibitor, for 3.5 h, and they were then evaluated by Western blotting. Data are presented as mean ± SEM. Two-way ANOVA, $*p < 0.05$ vs corresponding controls. **(B)** Western blot analysis demonstrating that YE-06-induced AMPK activation is dependent on LKB1 expression in HeLa cells. LKB1-deficient HeLa cells were transiently transfected with empty vector or LKB1 vector for 24 h. Time-dependent changes by YE-06 in the levels of AMPK-mediated signaling proteins were assessed by Western blotting. Data are presented as mean ± SEM. Two-way ANOVA, $**p < 0.01$ vs. control (empty or LKB1) **(C)** Immunofluorescence images showing YE-06-induced translocation of LKB1 from the nucleus to the cytoplasm. GST-LKB1 and DAPI are green and blue, respectively. Scale bars = 20 μm. The intensity of LKB1 was quantified using ImageJ (n = 5). Data are presented as the mean ± SEM. Statistical significance was determined using an unpaired two-tailed t-test. P < 0.01 vs. control.

YE-06 suppresses BACE1 expression and amyloidogenic processing through AMPK activation

Given that AD is characterized by multiple pathological hallmarks, including amyloid deposition and tau pathology [4, 29-33], we first investigated whether YE-06 could modulate amyloidogenic pathways. Using HEK293 cells stably expressing Swedish mutant amyloid precursor protein (APPswe), we evaluated the effect of YE-06 on extracellular Aβ production. Dot blot analysis revealed that YE-06 markedly reduced the level of secreted Aβ (Figure 4A). Consistently, YE-06 also decreased the level of soluble APPβ, a product generated during β-secretase (BACE1)-mediated APP cleavage (Figure 4A). Since BACE1 is the key enzyme initiating amyloidogenic APP processing, we also examined whether YE-06 regulates BACE1 expression through AMPK activation. Previous studies have reported that AMPK activation can suppress BACE1 expression; however, conflicting results have also been described [17, 34]. To clarify this relationship, BACE1 expression was assessed in cells transfected with recombinant AMPK constructs. Activated AMPK suppressed BACE1 expression at the transcriptional level, as evidenced by reductions in both BACE1 protein and mRNA levels in cells transfected with wild-type or constitutively active AMPKα1, while no such effect was observed in cells transfected with dominant-negative AMPKα1 (Supplementary Figure S3) Importantly, YE-06 suppressed BACE1 expression more effectively than the known AMPK activators 5-aminoimidazole-4-carboxamide ribonucleoside (AICAR) and metformin (Figure 4B). Consistent with these findings, YE-06 decreased BACE1 expression in HT22 neuronal cells in a dose- and time-dependent manner (Figure 4C-E). Collectively, these findings suggest that pharmacological activation of AMPK by YE-06 suppresses amyloidogenic APP processing through transcriptional downregulation of BACE1.

YE-06 suppresses microglial inflammatory signaling through the AMPK–SIRT1–NF-κB axis

Neuroinflammation driven by activated microglia is a key pathological feature of AD [30, 31]. Since activated AMPK has been reported to inhibit neuroinflammatory signaling [35], we evaluated whether YE-06 suppresses inflammatory responses in BV2 microglial cells. ELISA assay results showed that YE-06 significantly reduced lipopolysaccharide (LPS)-induced secretion of the pro-inflammatory cytokines IL-1β and TNF-α into the conditioned medium of BV2 cells (Figure 5A). Consistently, YE-06 also decreased the mRNA levels of *Il1b* and *Tnf*, which encode IL-1β and TNF-α, respectively (Figure 5B). Because AMPK/SIRT1 signaling is known to inhibit the transcriptional activity of nuclear factor-κB (NF-κB), a key regulator of IL-1β and TNF-α [36] as well as BACE1 [37], we next investigated whether YE-06 affects NF-κB activity. YE-06 inhibited the LPS-induced NF-κB activation, as evidenced by reduced nuclear localization of NF-κB (Figure 5C-D and Supplementary Figure S4A-B). In addition, YE-06 decreased NF-κB acetylation which is a consequence of deacetylation by SIRT1 (Figure 5E-F). Consistent with these findings, YE-06 also downregulated LPS-induced BACE1 mRNA expression (Figure 5G). Taken together, these findings suggest that YE-06 activates AMPK, which subsequently activates SIRT1, leading to NF-κB deacetylation and reduced nuclear accumulation of NF-κB. This cascade ultimately suppresses the transcription of BACE1 and pro-inflammatory cytokines, such as IL-1β and TNF-α (Figure 5H).

YE-06 activates AMPK–Nrf2 antioxidant signaling and limits oxidative stress

Oxidative stress is another important pathogenic factor associated with neuroinflammation in AD. During inflammatory activation, microglia generate excessive reactive oxygen species (ROS), thereby contributing to neuronal damage [32, 33, 38]. Measurement of intracellular ROS levels using a DCFH-DA assay revealed that YE-06 significantly attenuated LPS-induced ROS production in BV2 microglial cells (Figure 6A). Nuclear factor erythroid 2-related factor 2 (Nrf2) is a key transcription factor regulating antioxidant-related genes such as *Hmox1* and *Nqo1*. Because AMPK has been reported to promote Nrf2 activation [39], we examined whether YE-06 modulates this pathway. YE-06 increased nuclear localization of Nrf2 (Figure 6B and Supplementary Figure S4C) and elevated the mRNA levels of *Hmox1* and *Nqo1* (Figure 6C). The results suggest that YE-06 activates AMPK and thereby promotes Nrf2-dependent antioxidant gene expression (Figure 6D).

Hyperactivated microglia release toxic mediators, including cytokines and ROS, which can induce neuronal apoptosis [40, 41]. To determine whether YE-06 protects neurons from microglia-derived neurotoxicity, HT22 neuronal cells were exposed to conditioned medium from LPS-stimulated BV2 cells. Exposure to conditioned medium from LPS-treated BV2 cells increased the levels of apoptotic markers, including cleaved caspase-3 and cleaved PARP, in HT22 cells. However, these effects were significantly reduced when BV2 cells had been co-

treated with LPS and YE-06 (Figure 6E). Similarly, HT22 cell viability was markedly reduced following exposure to conditioned medium from LPS-treated BV2 cells, whereas viability was substantially restored when the conditioned medium was derived from BV2 cells treated with both LPS and YE-06 (Figure 6F). Collectively, these results indicate that YE-06 alleviates oxidative stress and protects neurons from microglia-derived neurotoxicity.

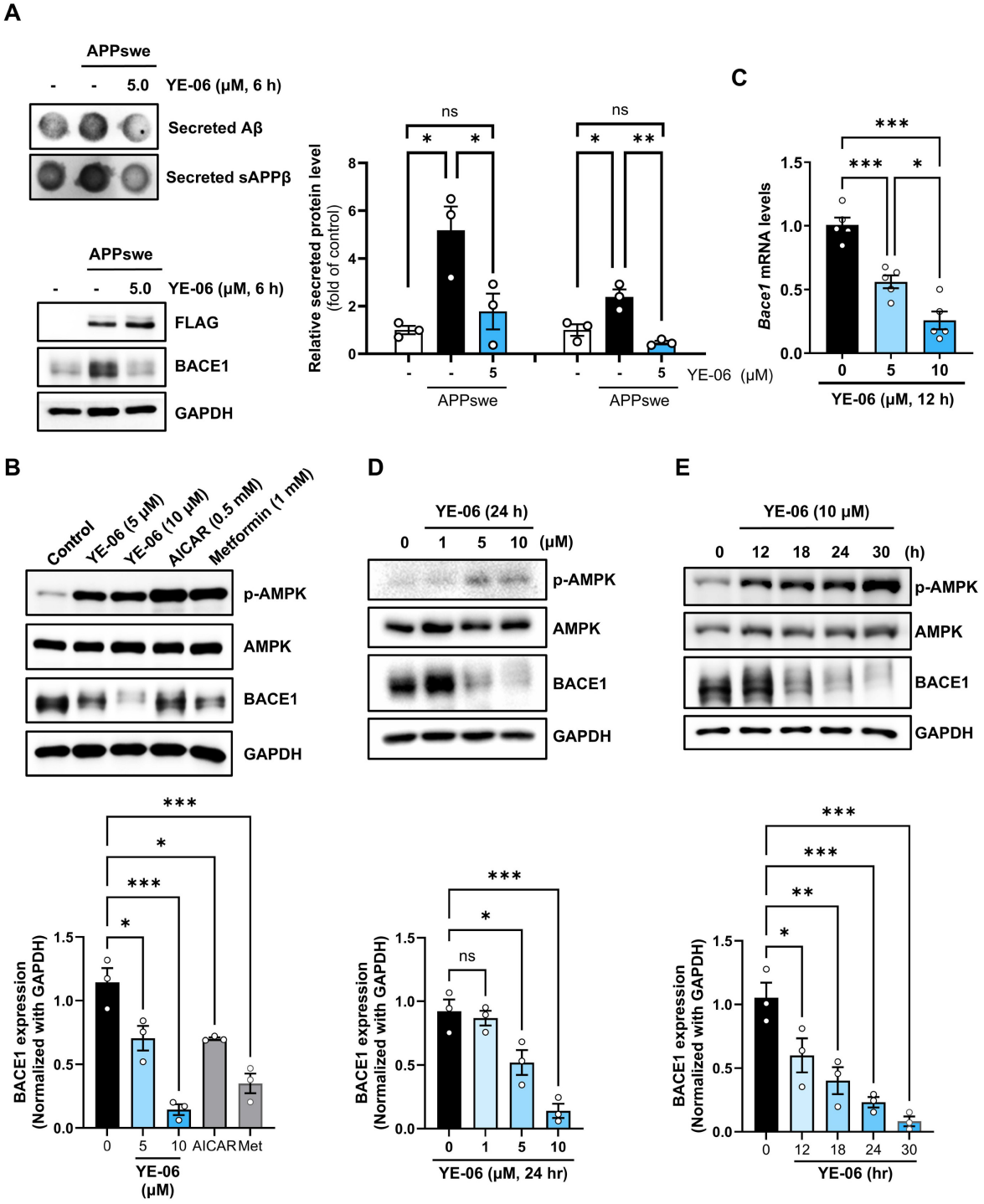


Figure 4. YE-06 suppresses BACE1 expression and amyloidogenic processing. (A) Western blot analysis of APP and BACE1 expression in HEK293-APPswe cells and dot blot analysis of secreted Aβ and sAPPβ in the conditioned medium collected from HEK293-APPswe cells grown with or without treatment of YE-06. Data are presented as mean ± SEM. Ordinary one-way ANOVA, *p < 0.05, **p < 0.01 vs. control. **(B)** Western blot analysis comparing the effects of AICAR, metformin, and YE-06 on AMPK activation and BACE1 expression in HT22 cells. Data are presented as mean ± SEM. Ordinary one-way ANOVA, *p < 0.05, ***p < 0.001 vs. control. **(C)** qRT–PCR analysis of BACE1 mRNA levels following YE-06 treatment for 12 h in HT22 cells (n = 5). Data are presented as mean ± SEM. Ordinary one-way ANOVA, *p < 0.05, ***p < 0.001. **(D, E)** Western blot analysis of dose-dependent **(D)** and time-dependent **(E)** effects of YE-06 on AMPK activation and BACE1 expression. Data are presented as mean ± SEM. Ordinary one-way ANOVA, *p < 0.05, **p < 0.01, ***p < 0.001 vs. control.

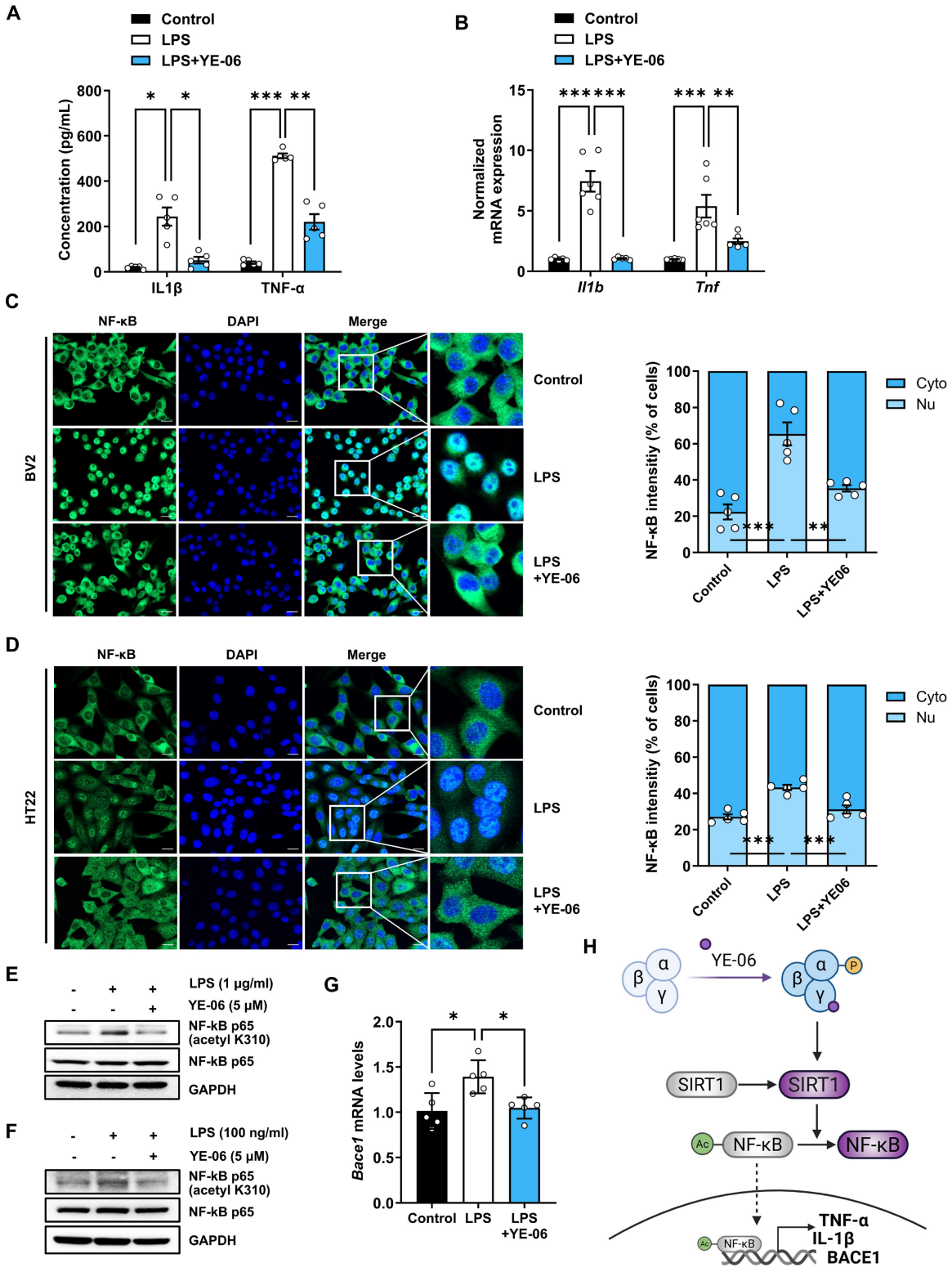


Figure 5. YE-06 suppresses microglial inflammatory signaling through the AMPK–SIRT1–NF-κB axis. (A) ELISA analysis showing reduced secretion of IL-1β and TNF-α in BV2 cells following YE-06 treatment. Cells were stimulated with LPS for 6 h in the absence or presence of YE-06 (5 μM), followed by medium replacement and further incubation for 24 h before collection of conditioned medium. YE-06 significantly reduced LPS-induced cytokine secretion (n = 5). Data are presented as mean ± SEM. Ordinary one-way ANOVA, *$p < 0.05$, **$p < 0.01$, ***$p < 0.001$ vs. LPS-only group. **(B)** qRT–PCR analysis showing reduced *Il1b* and *Tnf* expression following co-treatment of YE-06 and LPS for 12 h in BV2 cells (n = 5). Data are presented as mean ± SEM. Ordinary one-way ANOVA, **$p < 0.01$, ***$p < 0.001$ vs. LPS-only group. **(C, D)** Immunofluorescence images showing that YE-06 reduced LPS-induced nuclear translocation of NF-κB in BV2 **(C)** and HT22 **(D)** cells. Cells were pretreated with YE-06 for 11 h followed by LPS stimulation for 1 h. Scale bars = 20 μm. Fluorescence intensity was quantified using ImageJ, with intracellular NF-κB localization shown in the right panel. Data are presented as mean ± SEM. Ordinary one-way ANOVA, ***$p < 0.001$ vs. LPS-only group. **(E, F)** Western blot analysis showing reduced acetylation of NF-κB under the same treatment conditions in HT22 **(E)** and BV2 **(F)** cells. **(G)** qRT–PCR analysis of *Bace1* following co-treatment with YE-06 and LPS for 12 h in HT22 cells. Data are presented as mean ± SEM. Ordinary one-way ANOVA, *$p < 0.05$ vs. LPS-only group. **(H)** Schematic illustration of the proposed mechanism by which YE-06 activates AMPK/SIRT1 signaling, leading to NF-κB deacetylation, reduced nuclear localization, and subsequent suppression of *Bace1* transcription and pro-inflammatory cytokine expression.

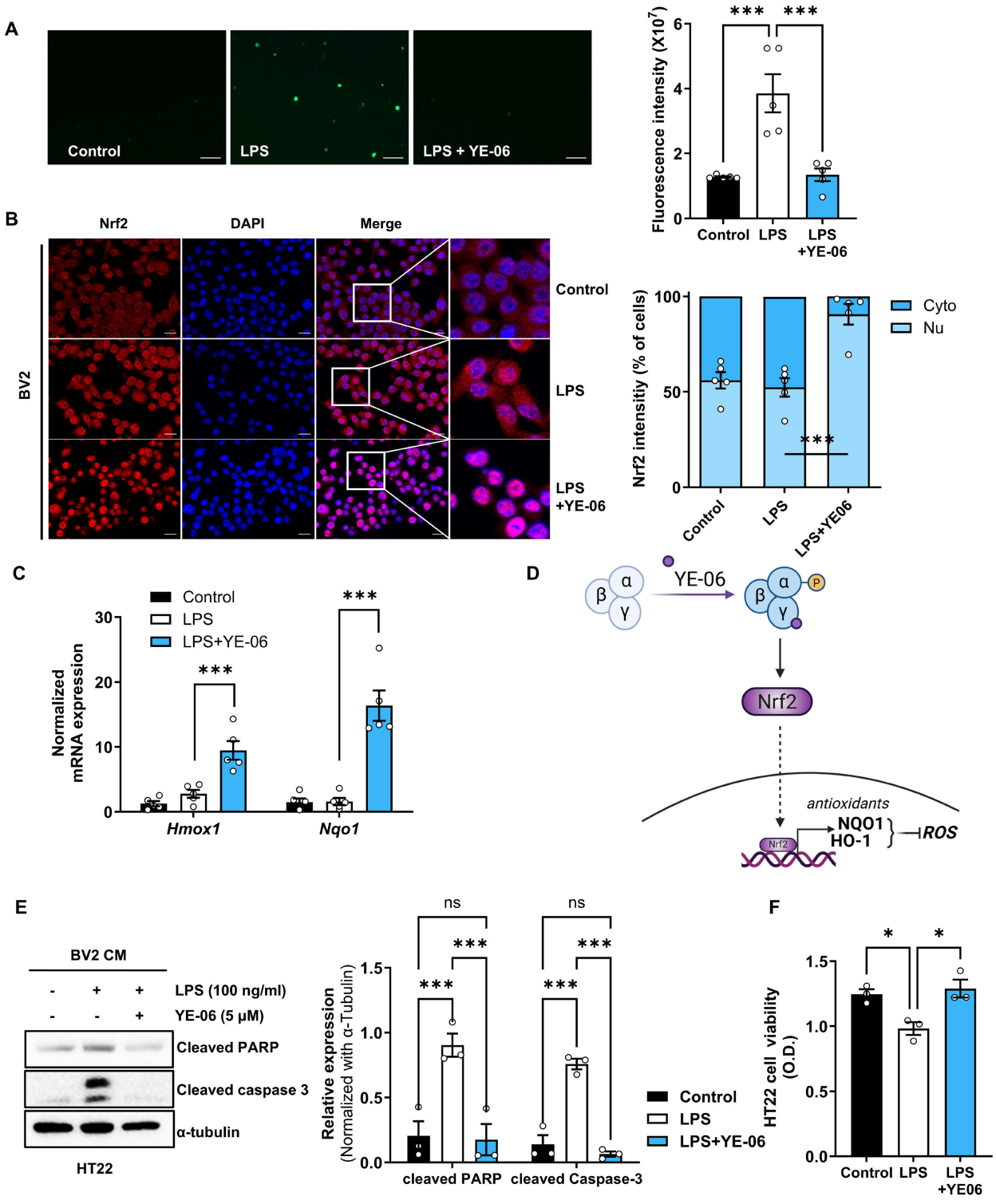


Figure 6. YE-06 activates the Nrf2 antioxidant pathway and confers neuroprotection. (A) Intracellular ROS levels in BV2 cells following LPS stimulation in the absence or presence of YE-06 (5 μM) were assessed by DCFH-DA fluorescence. YE-06 markedly reduced LPS-induced ROS production. Fluorescence intensity was quantified using ImageJ, and relative ROS levels are shown in the right panel (n = 5). Data are presented as mean ± SEM. Ordinary two-way ANOVA, ***p < 0.001 vs. LPS-only group. **(B)** Immunofluorescence analysis showing increased nuclear translocation of Nrf2 in BV2 cells following co-treatment with YE-06 and LPS for 12 h. Nrf2 (red) and nuclei (DAPI, blue) are shown. Scale bars = 20 μm. Fluorescence intensity of Nrf2 was quantified using ImageJ, and the intracellular distribution of Nrf2 is presented in the right panel. Data are presented as mean ± SEM. Ordinary two-way ANOVA, ***p < 0.001 vs. LPS-only group. **(C)** qRT–PCR analysis showing increased expression of antioxidant genes (*Hmox1* and *Nqo1*) following YE-06 treatment in BV2 cells. Data are presented as mean ± SEM (n = 3). Ordinary one-way ANOVA, ***p < 0.001 vs. LPS-treated control. **(D)** Schematic illustration showing that AMPK activation by YE-06 promotes Nrf2-dependent transcription, leading to increased expression of antioxidant genes and reduced ROS production. **(E)** Western blot analysis of apoptotic markers (cleaved PARP and cleaved caspase-3) in HT22 cells exposed to conditioned medium from BV2 cells treated with LPS in the absence or presence of YE-06. BV2 cells were stimulated with LPS for 6 h in the absence or presence of YE-06 (5 μM), followed by medium replacement and further incubation for 24 h before collection of conditioned medium. **(F)** Cell viability assay showing that YE-06 attenuates microglia-derived neurotoxicity in HT22 cells. HT22 cells were incubated for 72 h with conditioned medium from BV2 cells that had been stimulated with LPS for 12 h in the absence and presence of YE-06. Cell viability was assessed using a WST-1 assay. Data are presented as mean ± SEM (n = 3). Ordinary one-way ANOVA. *p < 0.05 vs. LPS-only group.

YE-06 improves cognition and neuronal function in Aβ$_{1-42}$-injected and 3xTg-AD mouse models

We next evaluated the behavioral effects of YE-06 in an intrahippocampal Aβ$_{1-42}$ injection model, a widely used experimental model for AD study [42]. In the Morris water maze test, mice treated with YE-06 at 10 and 100 mg/kg showed improved spatial learning during training sessions, comparable to that observed in donepezil-treated mice (Figure 7A-B), and enhanced short-term and long-term memory retention in subsequent trials (Supplementary Figure S5). In the probe test, mice treated with YE-06 at 10 mg/kg demonstrated a significant alleviation of Aβ$_{1-42}$-induced memory impairment, indicating improved long-term spatial memory retention (Figure 7C-D). In addition, the passive avoidance test showed significant improvement in contextual memory in the YE-06-treated group (100 mg/kg) (Figure 7E). Locomotor performance did not differ between groups in the vertical pole and the rotarod tests (Figure 7F-G), indicating that the behavioral improvements were attributable to cognitive enhancement rather than altered motor function.

Biochemical analysis of hippocampal tissues showed that YE-06 increased acetylcholine levels and decreased acetylcholinesterase activity (Figure 7H-I), with effects comparable to those observed with donepezil. Notably, unlike donepezil, YE-06 significantly suppressed Aβ$_{1-42}$-induced cell death (Figure 7J), consistent with previous findings of cytoprotective effects of AMPK activation [43].

The behavioral efficacy of YE-06 was further confirmed in the 3xTg-AD mouse model. Following a 12-week oral treatment regimen (Figure 8A), a novel object recognition (NOR) test was performed to assess episodic memory (Figure 8B). Administration of YE-06 resulted in a significantly higher discrimination index compared with the vehicle-treated group (Figure 8C), indicating improved recognition memory. Subgroup analyses demonstrated that YE-06 improved NOR performance in both male and female 3xTg-AD mice, indicating that its cognitive benefit was observed in both sexes (Supplementary Figure S6A). No significant differences in body weight or food consumption were observed between vehicle- and YE-06-treated mice throughout the treatment period (Supplementary Figure S6B & C). To further evaluate the multi-domain cognitive effects of YE-06, frontal/executive function was assessed using touchscreen-based behavioral testing (Figure 8D). Attention was measured using the five-choice serial reaction time task (5-CSRTT) (Figure 8E). After training, 10-month-old 3xTg-AD mice that achieved greater than 80% accuracy at a 2 s stimulus duration (baseline) were subjected to a probe session with increased task difficulty (0.5 s stimulus duration). Under these challenging conditions, YE-06 significantly enhanced attentional performance, as indicated by increased accuracy (Figure 8F), without affecting omission rates (Figure 8G). Importantly, YE-06 did not affect inhibitory control or locomotor activity, as premature responses, perseverative responses, beam breaks, and response latencies did not differ between groups (Figure 8H-J and Supplementary Figure S7).

To examine the contribution of AMPK signaling to attentional performance, baseline behavioral performance was first confirmed to be comparable between groups (Supplementary Figure S8A-E). During the subsequent probe phase, pharmacological inhibition of AMPK with Compound C significantly reduced response accuracy and increased premature responses in 15-month-old C57BL/6 mice, whereas omission rates, response latency, reward collection latency, perseverative responses, and beam breaks remained unchanged (Supplementary Figure S8F-M), supporting the involvement of AMPK signaling in attentional regulation. Electrophysiological analysis further supported the functional efficacy of YE-06. YE-06 enhanced neuronal excitability, as reflected by an increased number of action potential spikes, without altering resting membrane potential, spike amplitude, input resistance, or time taken for first spike (Figure 8K-Q). In addition, YE-06 increased the expression of synaptic and neuronal markers, including synaptophysin and MAP-2, in mouse primary neuron culture (Supplementary Figure S9). Collectively, these findings indicate that YE-06 improves multiple cognitive domains and enhances neuronal function in AD models, supporting its potential as a disease-modifying therapeutic strategy targeting AMPK signaling.

YE-06 exhibits favorable pharmacological properties

In addition to efficacy of YE-06 *in vitro* and *in vivo* models, YE-06 exhibited pharmacologically favorable properties supporting its further therapeutic applications. YE-06 demonstrated low cytotoxicity in various normal mammalian cell lines, including VERO, HFL-1, L929, NIH-3T3, and CHO-K1 cells, with IC_{50} values exceeding 100 μM in most tested cell types (Figure 9A). Also, safety assessment indicated that YE-06 did not exhibit mutagenic activity in the Ames test and showed no detectable inhibition of hERG potassium channel, which suggests a low risk of genotoxicity and cardiotoxicity (Figure 9B-D). Pharmacokinetic analysis showed favorable oral pharmacokinetic properties of YE-06. Notably, oral

administration of YE-06 resulted in high bioavailability (76.06%), indicating efficient systemic exposure following oral dosing (Figure 9E). The repeated oral administration produced significant cognitive improvements in both Aβ1-42-injected and 3xTg-AD mouse models without affecting locomotor activity or causing significant signs of toxicity (Figure 7 and 8).

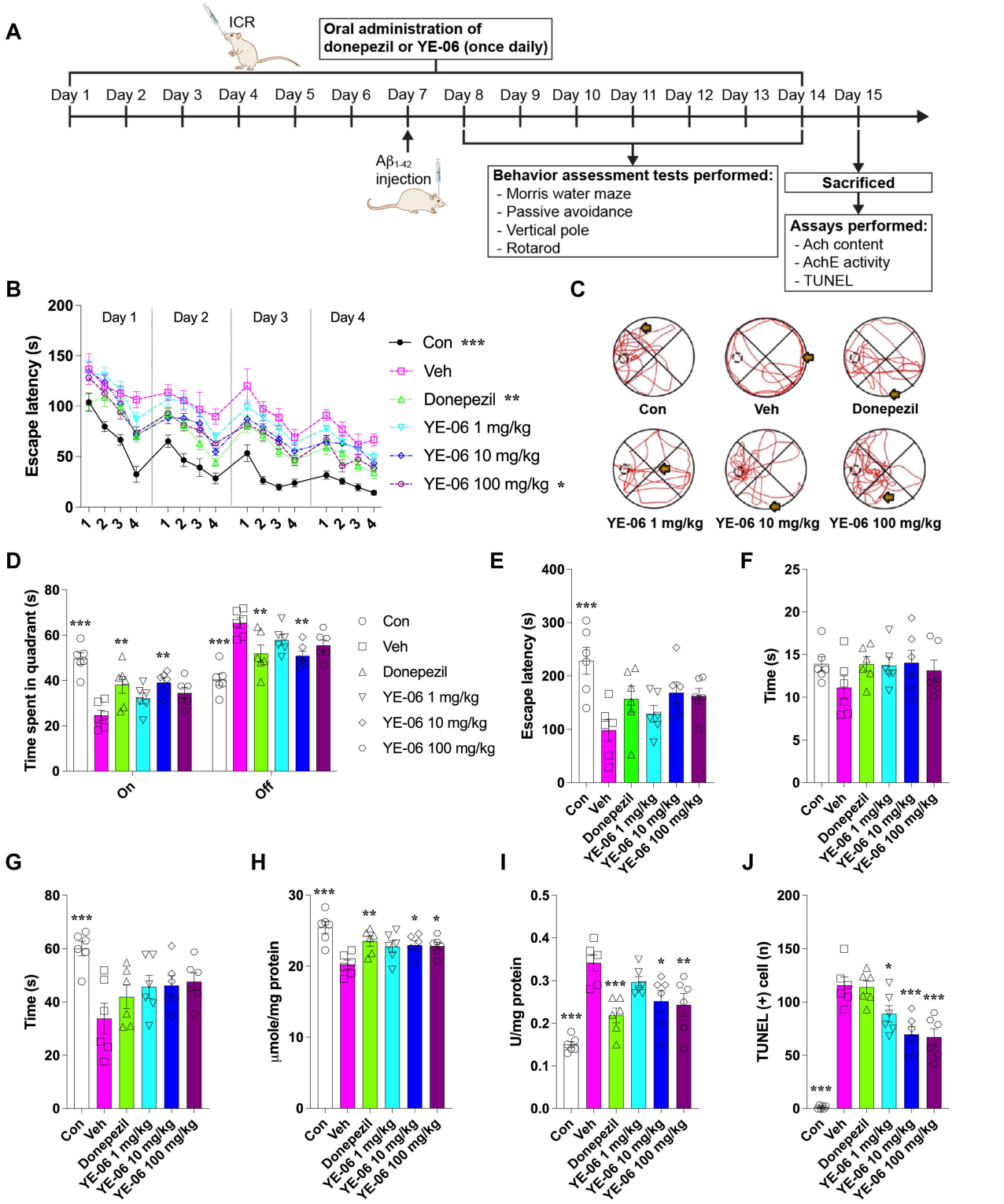


Figure 7. YE-06 improves cognitive performance and reduces neuronal damage in Aβ1–42-injected mice. (A) Experimental timeline. Aβ1-42-injected mice received daily oral administration of vehicle (Veh), donepezil (1 mg/kg), or YE-06 (1 mg/kg, 10 mg/kg, or 100 mg/kg) for 14 days. Behavioral testing was performed in 7–8-week-old ICR mice. **(B)** Escape latency during the acquisition phase of the Morris water maze test (n = 6). **(C)** Representative swimming paths during the probe trial, shown using a smart video tracking system. **(D)** Time spent in on-target and off-target quadrants during the probe trial (n = 6). **(E)** Passive avoidance test showing latency time (n = 6). **(F, G)** Motor function was assessed by vertical pole **(F)** and rotarod **(G)** tests (n = 6). **(H-J)** Neurochemical and histological analyses showing acetylcholine levels (**H**, n = 6),

acetylcholinesterase activity (**I**, n = 6), and TUNEL-positive cells (**J**, n = 6). Data are presented as mean ± SEM. One-way ANOVA and two-way mixed-effects model with Dunnett's multiple comparison post-hoc test. *$p < 0.05$, **$p < 0.01$, ***$p < 0.001$ *vs.* Veh. Con, Aβ1-42 non-injected and drug-nontreated mice; Veh, $A\beta_{1\text{-}42}$ injected and drug-nontreated mice.

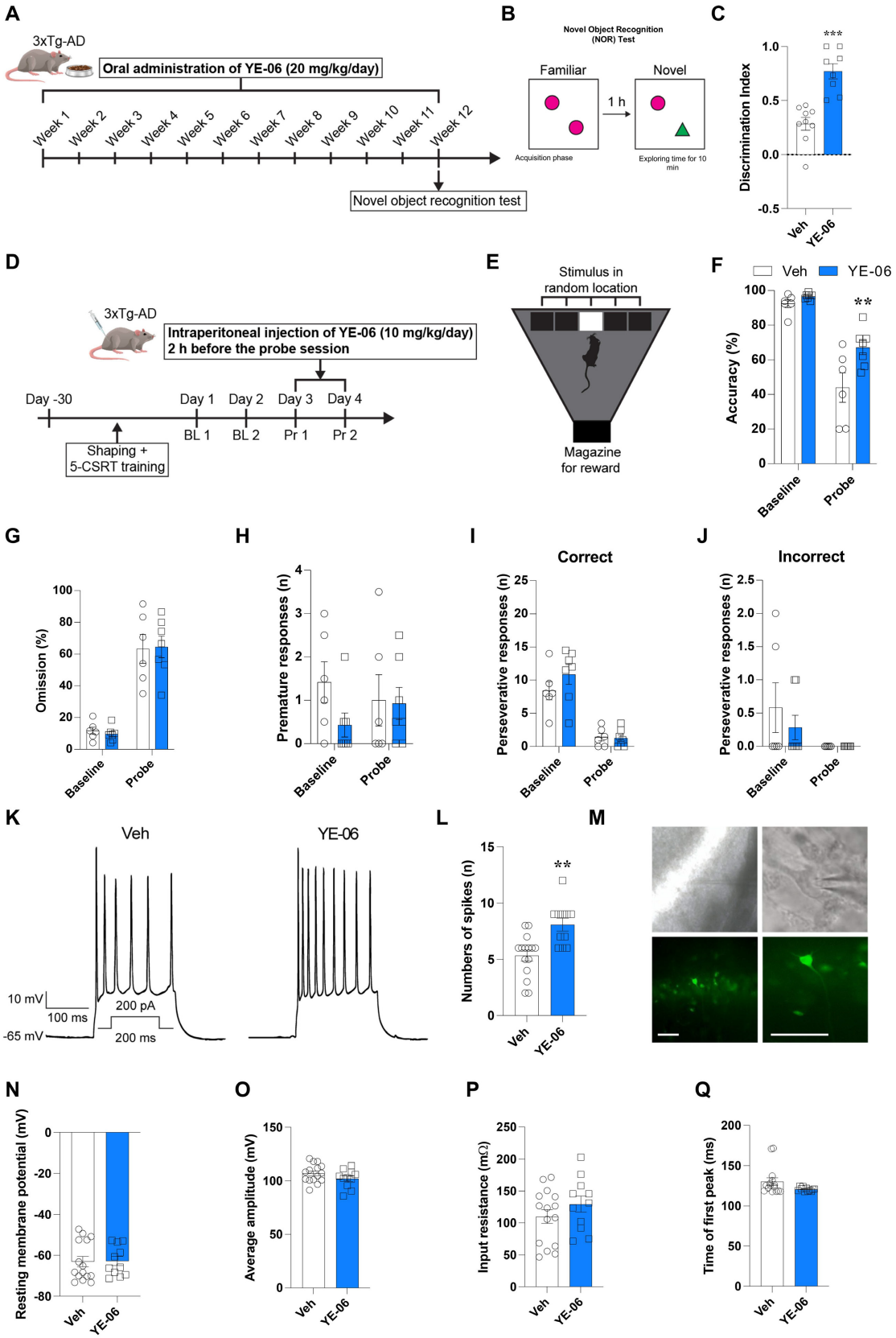


Figure 8. YE-06 improves cognitive function and neuronal excitability in 3xTg-AD mice. (A) Experimental timeline of the novel object recognition (NOR) test. NOR testing was performed in 9- or 12-month-old 3xTg-AD mice following 12 weeks of oral administration of vehicle (Veh, n = 9) or YE-06 (20 mg/kg, n = 8). **(B)** Schematic

of the NOR test. **(C)** Discrimination index calculated as (time exploring novel object − familiar object) / total exploration time. **(D, E)** Experimental timeline **(D)** and schematic **(E)** of the five-choice serial reaction time task (5-CSRTT). **(F-J)** Attentional performance and inhibitory control assessed during the probe session (0.5 s SD) in 10-month-old 3xTg-AD mice treated with vehicle (n = 6) or YE-06 (10 mg/kg, n = 7) for 2 h. Parameters include accuracy **(F)**, omission **(G)**, premature responses **(H)**, and perseverative responses to correct **(I)** and incorrect **(J)** stimuli. **(K-Q)** Electrophysiological recordings from hippocampal CA1 pyramidal neurons in brain slices from C57BL/6 mice. Following a single current injection (200 pA, 200 ms; Veh, n = 15 cells from 7 mice; YE-06, n = 11 cells from 6 mice), representative response **(K)** and numbers of spikes **(L)** were obtained. Representative bright-field images (4× and 40×) and streptavidin staining confirming recorded CA1 pyramidal neurons are shown (**M**; scale bar, 50 μm). Additional membrane properties, including resting membrane potential **(N)**, average amplitude **(O)**, total input resistance **(P)**, and time taken for the first peak **(Q)**, were analyzed. Data are shown as mean ± SEM. Unpaired Student's *t*-test. $^{**}p < 0.01$, $^{***}p < 0.001$ *vs.* Veh. Veh, vehicle.

A

IC50 (μM) in various normal mammalian cells				
VERO	HFL-1	L929	NIH 3T3	CHO-K1
83.6	>100	>100	>100	>100

B

Acute toxicity
Lethality: 0% (n=3 male & n=3 female ICR mice aged 9 weeks, 1000mg/kg)

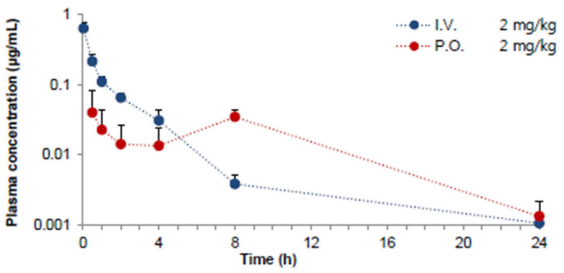
C

Tester strain	Compound	Dose (μg/plate)	Revertant colonies/plate (Mean ± SD) [Factor]	
			w/o S-9 mix	w S-9 mix
TA98	Vehicle control	0	19 ± 2	23 ± 2
	YE-06	200	20 ± 4[1.1]	35 ± 2[1.5]
TA100	Vehicle control	0	112 ± 16	111 ± 5
	YE-06	200	104 ± 12[0.9]	117 ± 4[1.0]

D

Treatment	Concentration (μM)	% inhibition
Astemizole (positive control)	10	69.4 ± 4.78
YE-06	10	< 1

E



Parameters	I.V. 2mg/kg	P.O. 2mg/kg
T_{max} (h)	NA	5.5 ± 4.33
C_{max} (μg/mL)	NA	0.049 ± 0.033
$T_{1/2}$ (h)	3.48 ± 0.14	3.73 ± 0.54
AUC_t (μg·h/mL)	0.605 ± 0.096	0.461 ± 0.155
AUC_∞ (μg·h/mL)	0.611 ± 0.096	0.468 ± 0.152
CL (L/h/kg)	3.32 ± 0.48	NA
V_{ss} (L/kg)	7.41 ± 1.68	NA
F_t (%)	NA	76.06

NA, not applicable; not detected; NC, not calculated

F

Solubility (Kinetic)	Log P	Permeability
206.2 ± 1.7 μM (94.4 ± 0.8 μg/ml)	4.75	-4.4 ± 0.152 (grade: medium)

G

Comp. \ Isoform	IC50 (μM)						
	1A2	2B6	2C8	2C9	2C19	2D6	3A4
YE-06	4.44	>10 (13.63)	3.46	0.0460	6.13	>10	>10
Reference*	0.00410	0.863	0.170	0.587	2.25	0.0246	0.0325

*CYP1A2: a-Naphthoflavone; CYP2C9: Sulfaphenazole; CYP2C19: Omeprazole;CYP3A4: Ketoconazole;CYP2D6: Quinidine; CYP2C8:Montelukast ; CYP2B6:Ticlopidine

H

Test Article	$t_{1/2}$ (minute)	CL_{int} (mL/min/kg)	CLh (mL/min/kg)	Eh(%)
YE-06	62.57	27.78	11.86	57.30

I

Time (h)	YE-06 (ng/mL)	
	Plasma	Brain
0.05	1740.54	3136.04
0.25	1212.14	2236.21
0.5	453.63	1081.68
1	220.76	529.94
2	25.71	64.85
4	2.30	14.41
8	0.41	13.36

	YE-06	
	Plasma	Brain
$T_{1/2}$ (h)	0.653	0.985
AUC_last (h*ng/mL)	919.9	1950.8
AUC_inf (h*ng/mL)	920.3	1969.8
CL (L/h/kg)	10.9	0.0152
Vss (L/kg)	5.25	0.0116
B/P ratio	2.1	

Figure 9. Evaluation of YE-06 druggability. (A, B) Cytotoxicity of YE-06 was assessed in various normal mammalian cell lines (A) and mice (B). **(C)** Genotoxicity of YE-06 was evaluated through Ames test. **(D)** Cardiac toxicity was measured by hERG K^+ channel binding assay. **(E)** Pharmacokinetic profiles of YE-06 were evaluated at each of the indicated doses. The extract of the plasma sample was analyzed using LC-MS/MS. **(F)** Kinetic solubility and log P were determined through nephelometry and the pH-metric method. Permeability was evaluated with a PAMPA assay. **(G)** CYP inhibition of YE-06 was evaluated against major CYP isoforms, including CYP1A2, CYP2B6, CYP2C8, CYP2C9, CYP2C19, CYP2D6, and CYP3A4. **(H)** Metabolic stability of YE-06 was evaluated using liver microsomes. **(I)** Brain distribution of YE-06 was evaluated following intraperitoneal administration (10 mg/kg), and brain and plasma concentrations were determined using LC-MS/MS.

YE-06 also showed acceptable physiochemical properties, including moderate permeability, favorable solubility and a drug-like logP value (Figure 9F). CYP inhibition profiling revealed differential inhibitory effects of YE-06 across major CYP isoforms. YE-06 showed the strongest inhibition of CYP2C9 (IC_{50} = 0.046 μM), while moderate inhibition was observed for CYP1A2, CYP2C8, and CYP2C19 (IC_{50} = 4.44, 3.46, and 6.13 μM, respectively). In contrast, relatively weak or minimal inhibition was observed

for CYP2B6, CYP2D6, and CYP3A4 (IC_{50} > 10 μM) (Figure 9G). YE-06 also exhibited favorable metabolic stability in microsomal assays (Figure 9H).

Importantly, brain pharmacokinetic analysis demonstrated that YE-06 effectively reached the brain following systemic administration. YE-06 achieved substantial brain exposure with a brain-to-plasma ratio of 2.1, supporting efficient brain penetration and its potential as a CNS-targeting therapeutic agent (Figure 9I). Collectively, these findings demonstrate favorable pharmacokinetic, metabolic stability, and CNS exposure profiles of YE-06, while the potent CYP2C9 inhibition identified in the CYP profiling warrants further evaluation during subsequent development.

Discussion

AD is a multifactorial neurodegenerative disorder characterized by progressive cognitive decline and pathological hallmarks, including Aβ accumulation, neuroinflammation, and oxidative stress [44, 45]. In this study, we identified YE-06 as a direct activator of AMPK and demonstrated that pharmacological activation of AMPK by YE-06 mitigates multiple pathological processes associated with AD. YE-06 directly interacts with the AMPKγ subunit, specifically at the CBS3 site, thereby activating downstream signaling and exerting neuroprotective effects against amyloid pathology, neuroinflammation, oxidative stress, and cognitive impairment in both cellular and animal models of AD.

To investigate the mechanism underlying AMPK activation, we examined the direct interaction between YE-06 and AMPK using CETSA, a widely used label-free technique that monitors changes in thermal stability induced by ligand binding to endogenous target proteins within cells [20]. This analysis confirmed that YE-06 binds to the CBS3 site of the AMPKγ subunit, consistent with our molecular docking results. Site-directed mutagenesis further showed that this interaction depends on residues His298 and Arg299, providing structural insight into the activation mechanism of YE-06. In our previous study [19], *in vitro* kinase assays performed in the absence of upstream kinases demonstrated that YE-06 directly enhances AMPK enzymatic activity, supporting its function as a direct AMPK activator. Interestingly, however, cellular experiments revealed that YE-06-induced AMPK phosphorylation remains dependent on the upstream kinase LKB1. These observations suggest a synergistic model where the direct binding of YE-06 initiates AMPK activation and may induce a conformational change that facilitates or stabilizes LKB1-mediated phosphorylation, ensuring sustained AMPK signaling.

The accumulation of extracellular Aβ peptides, generated through sequential cleavage of APP by BACE1 and γ-secretase, represents a central pathological feature of AD. Both insoluble Aβ and soluble sAPPβ levels are much higher in the brains of AD patients compared to non-AD and disease control cases [46]. Consistent with this pathological mechanism, YE-06 reduced both Aβ and sAPPβ levels in APPswe-expressing cells. Mechanistically, AMPK activation by YE-06 suppresses BACE1 expression at the transcriptional level through modulating the AMPK–SIRT1–NF-κB signaling axis, suggesting that AMPK signaling may regulate amyloidogenic processing of APP. These findings are consistent with previous studies reporting that AMPK activation can suppress BACE1 expression and reduce Aβ production [34].

Beyond amyloid pathology, neuroinflammation has emerged as a major contributor to AD progression. Hyperactivated microglia release inflammatory mediators such as IL-1β, TNF-α and ROS, which exacerbate neuronal damage and cognitive impairment [40, 41]. In the present study, YE-06 attenuates LPS-induced inflammatory responses and reduces the production of neurotoxic mediator in microglial cells. Mechanistically, these effects are associated with the simultaneous suppression of NF-κB signaling and activation of the Nrf2 antioxidant pathway. Through this coordinated regulation, AMPK activation by YE-06 coordinately modulates several key pathological processes involved in AD, including amyloidogenesis, neuroinflammation, and oxidative stress.

The therapeutic relevance of these molecular effects was supported by behavioral experiments. In the intrahippocampal $Aβ_{1–42}$ injection model, YE-06 significantly improves spatial learning and memory retention. Furthermore, in the 3xTg-AD mouse model, YE-06 enhances recognition memory and attentional performance without altering baseline locomotor activity. These findings demonstrate that YE-06 improves multiple cognitive domains in AD models. Notably, YE-06 improved recognition memory in both male and female 3xTg-AD mice (Supplementary Figure S6A), indicating that its cognitive benefit was observed in both sexes. The behavioral paradigms employed different treatment schedules: recognition memory was evaluated after 12 weeks of oral YE-06 administration in chow, whereas attentional performance in the 5-CSRTT was assessed 2 h after intraperitoneal administration before each probe session. The attentional benefit is therefore consistent with a short-term pharmacological effect, potentially involving neuromodulation, although a contribution from repeated exposure cannot be excluded. These

findings should not be interpreted as evidence of disease modification, and whether the attentional effects share the mechanisms underlying the benefits observed after chronic oral treatment remains to be determined. Interestingly, although YE-06 significantly improved behavioral outcomes in the 3xTg-AD mice, these beneficial effects were not accompanied by increased AMPK phosphorylation in the hippocampus at the corresponding behavioral endpoints (Supplementary Figure S10). Instead, reduced AMPK phosphorylation was observed in both experimental cohorts. AMPK phosphorylation is dynamically regulated according to cellular energy status, and its level at a single endpoint may not necessarily reflect the overall extent of AMPK pathway engagement [47, 48]. Consistent with this notion, previous studies have reported that treatment with the established AMPK activator, AICAR, did not increase hippocampal AMPK phosphorylation at the examined time point [8]. One possible explanation for the reduction observed after YE-06 treatment is secondary metabolic adaptation associated with changes in cellular energy homeostasis; however, the present endpoint measurements cannot establish this mechanism. Supporting this possibility, YE-06 increased ATP levels and reduced the ADP/ATP ratio in N2a cells (Supplementary Figure S2E), providing evidence of altered cellular energy status in vitro, but not direct evidence of metabolic adaptation in the brain. Moreover, despite the reduced hippocampal AMPK phosphorylation at the terminal endpoint, YE-06 produced favorable changes in AD-related molecular markers, including decreased BACE1 expression and reduced tau phosphorylation. These findings support the beneficial molecular effects of YE-06 *in vivo*, but do not independently establish brain AMPK target engagement or explain the reduction in AMPK phosphorylation observed at the terminal endpoint. Further time-course studies will be required to characterize the temporal relationship between AMPK activation, metabolic adaptation, and the downstream therapeutic effects of AMPK activators in the AD brain.

YE-06 also demonstrated favorable drug-like properties supporting its translational potential. YE-06 exhibited high oral bioavailability (76%). In a separate brain distribution study following intraperitoneal administration, YE-06 showed substantial brain exposure, with a brain-to-plasma ratio of 2.1, supporting its ability to reach the brain following systemic administration. In addition, YE-06 showed favorable microsomal stability and limited inhibition of most major CYP isoforms. However, YE-06 potently inhibited CYP2C9 (IC_{50} = 0.046 μM), indicating a potential drug-drug interaction liability given the plasma Cmax observed following oral administration in mice (0.049 μg/mL, approximately 100 nM). Further studies incorporating unbound exposure, inhibition kinetics, and metabolite characterization will be required to assess the clinical relevance of this interaction. Furthermore, preliminary safety evaluation demonstrated no acute toxicity, negative Ames test results, and no detectable hERG channel inhibition. Collectively, these findings support a favorable pharmacokinetic and preliminary safety profile of YE-06, while the observed CYP2C9 inhibition warrants further evaluation during subsequent preclinical development.

Nevertheless, several limitations should be considered. Although YE-06 directly activated AMPK in the experimental systems used in this study, additional work is required to comprehensively evaluate its potential off-target effects and long-term safety. Furthermore, future studies should assess the therapeutic efficacy of YE-06 in additional AD models and further characterize its pharmacokinetic and pharmacodynamic properties.

Several direct AMPK activators are currently undergoing preclinical and clinical evaluation. For example, PXL770 (NCT03763877) and O403 (EudraCT 2016-002183-13) have reached Phase II clinical trials for the treatment of non-alcoholic fatty liver disease and type II diabetes, respectively. Most direct AMPK activators target either the ADaM site or the nucleotide-binding sites within the AMPKγ subunit [49-51]. However, targeting CBS sites remains challenging due to their structural similarity to endogenous nucleotides and the associated risk of off-target effects. In this context, YE-06 represents a distinct class of AMPK activators that engages the CBS3 site through a non-nucleotide-mimetic scaffold. This structural divergence from traditional nucleotide mimetics may offer a pharmacological advantage by providing an alternative strategy for direct AMPK activation without structural mimicry of endogenous nucleotides.

In summary, this study introduces YE-06 as a novel, orally available direct AMPK activator that directly binds to the AMPKγ subunit through a CBS3-dependent interaction. YE-06 modulates multiple disease-relevant pathways, including suppression of BACE1-dependent amyloidogenesis and attenuation of neuroinflammatory and oxidative stress responses through the regulation of the NF-κB and Nrf2 pathways. These molecular effects translate into significant cognitive improvements in two independent AD mouse models. Collectively, our discovery and characterization of YE-06 highlight its potential as a novel therapeutic strategy for AD treatment. By effectively modulating key pathological

processes and providing neuroprotection, YE-06 represents a promising candidate for further clinical development in the quest of overcoming AD.

Supplementary Material

Supplementary materials and methods, figures and tables. https://www.ijbs.com/v23p0270s1.pdf

Acknowledgements

Graphical abstract and mechanistic schemes were created with BioRender.com.

Funding

This study was supported by grants from the Bio & Medical Technology Development Program of the National Research Foundation (NRF) funded by the Korean government (Ministry of Science and ICT) (2022R1A2C2092053, RS-2024-00431505), and the Ministry of Health and Welfare (HR22C141102), and a faculty research grant from Yonsei University College of Medicine (6-2022-0053).

Data availability statement

The data that support the findings of this study are available from the corresponding author upon reasonable request.

Authorship contribution statement

Kyung-Hwa Jeon: Validation, Investigation, Writing-Original Draft, Visualization. **Hyunji Jo:** Investigation, Visualization. **Soyeon Cho:** Investigation, Visualization. **Jae-Ho Shin:** Investigation. **Seojeong Park**: Investigation. **Kyu-Yeon Jun:** Investigation. **Seojeong Kim:** Investigation. **Seung Hee Seo:** Investigation. **Soo-Yeon Hwang:** Investigation. **Dabin Song:** Investigation. **Yumi Son:** Investigation. **Zhi Zheng**: Investigation. **Hyunjeong Kim:** Investigation. **Younghwa Na:** Writing- Review and Editing. **Eosu Kim:** Writing- Review and Editing, Funding acquisition. **Youngjoo Kwon:** Conceptualization, Supervision, Writing-Review and Editing, Funding acquisition.

AI usage Statement

ChatGPT (OpenAI) was used to assist with the development and debugging of R and Python scripts for bioinformatics data analysis, as well as English language editing and improvements in manuscript readability. All AI-assisted outputs were reviewed by the authors, who take full responsibility for the accuracy and integrity of the manuscript.

Competing Interests

Some of the authors have applied for or hold patents for YE-06.

References

1. Sims JR, Zimmer JA, Evans CD, Lu M, Ardayfio P, Sparks J, et al. Donanemab in Early Symptomatic Alzheimer Disease: The TRAILBLAZER-ALZ 2 Randomized Clinical Trial. Jama. 2023; 330: 512–27.
2. van Dyck CH, Swanson CJ, Aisen P, Bateman RJ, Chen C, Gee M, et al. Lecanemab in Early Alzheimer's Disease. N Engl J Med. 2023; 388: 9–21.
3. Avgerinos KI, Manolopoulos A, Ferrucci L, Kapogiannis D. Critical assessment of anti-amyloid-β monoclonal antibodies effects in Alzheimer's disease: a systematic review and meta-analysis highlighting target engagement and clinical meaningfulness. Sci Rep. 2024; 14: 25741.
4. Gong C-X, Liu F, Iqbal K. Multifactorial hypothesis and multi-targets for Alzheimer's disease. Journal of Alzheimer's Disease. 2018; 64: S107–S17.
5. Cummings J, Lee G, Nahed P, Kambar MEZN, Zhong K, Fonseca J, et al. Alzheimer's disease drug development pipeline: 2022. Alzheimer's & Dementia: Translational Research & Clinical Interventions. 2022; 8: e12295.
6. Ge Y, Zhou M, Chen C, Wu X, Wang X. Role of AMPK mediated pathways in autophagy and aging. Biochimie. 2022; 195: 100–13.
7. Reznick RM, Zong H, Li J, Morino K, Moore IK, Yu HJ, et al. Aging-associated reductions in AMP-activated protein kinase activity and mitochondrial biogenesis. Cell Metab. 2007; 5: 151–6.
8. Jang S, Kim H, Jeong J, Lee SK, Kim EW, Park M, et al. Blunted response of hippocampal AMPK associated with reduced neurogenesis in older versus younger mice. Prog Neuropsychopharmacol Biol Psychiatry. 2016; 71: 57–65.
9. Salminen A, Kaarniranta K, Haapasalo A, Soininen H, Hiltunen M. AMP-activated protein kinase: a potential player in Alzheimer's disease. J Neurochem. 2011; 118: 460–74.
10. Vingtdeux V, Chandakkar P, Zhao H, d'Abramo C, Davies P, Marambaud P. Novel synthetic small-molecule activators of AMPK as enhancers of autophagy and amyloid-β peptide degradation. Faseb j. 2011; 25: 219–31.
11. Chen Y, Zhao S, Fan Z, Li Z, Zhu Y, Shen T, et al. Metformin attenuates plaque-associated tau pathology and reduces amyloid-β burden in APP/PS1 mice. Alzheimer's research & therapy. 2021; 13: 1–13.
12. Caberlotto L, Lauria M, Nguyen TP, Scotti M. The central role of AMP-kinase and energy homeostasis impairment in Alzheimer's disease: a multifactor network analysis. PLoS One. 2013; 8: e78919.
13. Park JS, Lee J, Jung ES, Kim M-H, Kim IB, Son H, et al. Brain somatic mutations observed in Alzheimer's disease associated with aging and dysregulation of tau phosphorylation. Nature communications. 2019; 10: 1–12.
14. Kim J, Yang G, Kim Y, Kim J, Ha J. AMPK activators: mechanisms of action and physiological activities. Experimental & molecular medicine. 2016; 48: e224–e.
15. Cho SY, Kim EW, Park SJ, Phillips BU, Jeong J, Kim H, et al. Reconsidering repurposing: long-term metformin treatment impairs cognition in Alzheimer's model mice. Transl Psychiatry. 2024; 14: 34.
16. Ha J, Choi DW, Kim KJ, Cho SY, Kim H, Kim KY, et al. Association of metformin use with Alzheimer's disease in patients with newly diagnosed type 2 diabetes: a population-based nested case-control study. Sci Rep. 2021; 11: 24069.
17. Son SM, Shin H-J, Byun J, Kook SY, Moon M, Chang YJ, et al. Metformin facilitates amyloid-β generation by β-and γ-secretases via autophagy activation. Journal of Alzheimer's Disease. 2016; 51: 1197–208.
18. Jeon KH, Park S, Pak ES, Kim JA, Liu Y, Hwang SY, et al. Calpain 2 Isoform-Specific Cleavage of Filamin A Enhances HIF1α Nuclear Translocation, Promoting Metastasis in Triple-Negative Breast Cancer. MedComm (2020). 2025; 6: e70147.
19. Jeon KH, Shin JH, Jo HJ, Kim H, Park S, Kim S, et al. Computer-aided discovery of novel AMPK activators through virtual screening and SAR-driven synthesis. Eur J Med Chem. 2025; 287: 117318.
20. Molina DM, Jafari R, Ignatushchenko M, Seki T, Larsson EA, Dan C, et al. Monitoring drug target engagement in cells and tissues using the cellular thermal shift assay. Science. 2013; 341: 84–7.
21. Xiao B, Sanders MJ, Underwood E, Heath R, Mayer FV, Carmena D, et al. Structure of mammalian AMPK and its regulation by ADP. Nature. 2011; 472: 230–3.
22. Yan Y, Zhou XE, Xu HE, Melcher K. Structure and physiological regulation of AMPK. International journal of molecular sciences. 2018; 19: 3534.
23. Gu X, Yan Y, Novick SJ, Kovach A, Goswami D, Ke J, et al. Deconvoluting AMP-activated protein kinase (AMPK) adenine nucleotide binding and sensing. Journal of Biological Chemistry. 2017; 292: 12653–66.
24. Langendorf CG, Ngoei KR, Scott JW, Ling NX, Issa SM, Gorman MA, et al. Structural basis of allosteric and synergistic activation of AMPK by furan-2-phosphonic derivative C2 binding. Nature communications. 2016; 7: 10912.
25. Hawley SA, Boudeau J, Reid JL, Mustard KJ, Udd L, Mäkelä TP, et al. Complexes between the LKB1 tumor suppressor, STRADα/β and MO25α/β are upstream kinases in the AMP-activated protein kinase cascade. Journal of biology. 2003; 2: 1–16.
26. Woods A, Dickerson K, Heath R, Hong S-P, Momcilovic M, Johnstone SR, et al. Ca2+/calmodulin-dependent protein kinase kinase-β acts upstream of AMP-activated protein kinase in mammalian cells. Cell metabolism. 2005; 2: 21–33.
27. Fulco M, Cen Y, Zhao P, Hoffman EP, McBurney MW, Sauve AA, et al. Glucose restriction inhibits skeletal myoblast differentiation by activating SIRT1

through AMPK-mediated regulation of Nampt. Developmental cell. 2008; 14: 661–73.
28. Cantó C, Jiang LQ, Deshmukh AS, Mataki C, Coste A, Lagouge M, et al. Interdependence of AMPK and SIRT1 for metabolic adaptation to fasting and exercise in skeletal muscle. Cell metabolism. 2010; 11: 213–9.
29. Forner S, Baglietto-Vargas D, Martini AC, Trujillo-Estrada L, LaFerla FM. Synaptic impairment in Alzheimer's disease: a dysregulated symphony. Trends in neurosciences. 2017; 40: 347–57.
30. Grammas P. Neurovascular dysfunction, inflammation and endothelial activation: implications for the pathogenesis of Alzheimer's disease. Journal of neuroinflammation. 2011; 8: 1–12.
31. Hansen DV, Hanson JE, Sheng M. Microglia in Alzheimer's disease. Journal of Cell Biology. 2018; 217: 459–72.
32. Huang WJ, Zhang X, Chen WW. Role of oxidative stress in Alzheimer's disease. Biomedical reports. 2016; 4: 519–22.
33. Simpson DS, Oliver PL. ROS generation in microglia: understanding oxidative stress and inflammation in neurodegenerative disease. Antioxidants. 2020; 9: 743.
34. Zhang H, Zhao C, Cao G, Guo L, Zhang S, Liang Y, et al. Berberine modulates amyloid-β peptide generation by activating AMP-activated protein kinase. Neuropharmacology. 2017; 125: 408–17.
35. Peixoto CA, de Oliveira WH, da Racho Araújo SM, Nunes AKS. AMPK activation: Role in the signaling pathways of neuroinflammation and neurodegeneration. Experimental neurology. 2017; 298: 31–41.
36. O'Neill LA, Kaltschmidt C. NF-kB: a crucial transcription factor for glial and neuronal cell function. Trends in neurosciences. 1997; 20: 252–8.
37. Buggia-Prevot V, Sevalle J, Rossner S, Checler F. NFkappaB-dependent control of BACE1 promoter transactivation by Abeta42. J Biol Chem. 2008; 283: 10037–47.
38. Vilhardt F, Haslund-Vinding J, Jaquet V, McBean G. Microglia antioxidant systems and redox signalling. British journal of pharmacology. 2017; 174: 1719-32.
39. Joo MS, Kim WD, Lee KY, Kim JH, Koo JH, Kim SG. AMPK Facilitates Nuclear Accumulation of Nrf2 by Phosphorylating at Serine 550. Mol Cell Biol. 2016; 36: 1931–42.
40. Wang W-Y, Tan M-S, Yu J-T, Tan L. Role of pro-inflammatory cytokines released from microglia in Alzheimer's disease. Annals of translational medicine. 2015; 3.
41. Kaur U, Banerjee P, Bir A, Sinha M, Biswas A, Chakrabarti S. Reactive oxygen species, redox signaling and neuroinflammation in Alzheimer's disease: the NF-κB connection. Current topics in medicinal chemistry. 2015; 15: 446–57.
42. Facchinetti R, Bronzuoli MR, Scuderi C. An animal model of Alzheimer disease based on the intrahippocampal injection of amyloid β-peptide (1–42). Neurotrophic Factors: Methods and Protocols. 2018: 343–52.
43. Ng CH, Guan MS, Koh C, Ouyang X, Yu F, Tan EK, et al. AMP kinase activation mitigates dopaminergic dysfunction and mitochondrial abnormalities in Drosophila models of Parkinson's disease. J Neurosci. 2012; 32: 14311–7.
44. DeTure MA, Dickson DW. The neuropathological diagnosis of Alzheimer's disease. Mol Neurodegener. 2019; 14: 32.
45. Long JM, Holtzman DM. Alzheimer Disease: An Update on Pathobiology and Treatment Strategies. Cell. 2019; 179: 312–39.
46. Chow VW, Mattson MP, Wong PC, Gleichmann M. An overview of APP processing enzymes and products. Neuromolecular medicine. 2010; 12: 1–12.
47. Hardie DG, Ross FA, Hawley SA. AMPK: a nutrient and energy sensor that maintains energy homeostasis. Nat Rev Mol Cell Biol. 2012; 13: 251–62.
48. McConell GK, Lee-Young RS, Chen ZP, Stepto NK, Huynh NN, Stephens TJ, et al. Short-term exercise training in humans reduces AMPK signalling during prolonged exercise independent of muscle glycogen. J Physiol. 2005; 568: 665–76.
49. Jørgensen NO, Kjøbsted R, Larsen MR, Birk JB, Andersen NR, Albuquerque B, et al. Direct small molecule ADaM-site AMPK activators reveal an AMPKγ3-independent mechanism for blood glucose lowering. Mol Metab. 2021; 51: 101259.
50. Aledavood E, Gheeraert A, Forte A, Vuillon L, Rivalta I, Luque FJ, et al. Elucidating the Activation Mechanism of AMPK by Direct Pan-Activator PF-739. Front Mol Biosci. 2021; 8: 760026.
51. Yan Y, Zhou XE, Novick SJ, Shaw SJ, Li Y, Brunzelle JS, et al. Structures of AMP-activated protein kinase bound to novel pharmacological activators in phosphorylated, non-phosphorylated, and nucleotide-free states. J Biol Chem. 2019; 294: 953–67.